




S,S-Chiral Linker Induced U Shape with a Syn-facial Sensitizer and Photocleavable Ethene Group[†]

Goutam Ghosh^{1,2,3}, Sarah J. Belh^{2,3}, Callistus Chiemezie^{2,3}, Niluksha Walalawela^{2,3}, Ashwini A. Ghogare^{2,3}, Mariana Vignoni⁴, Andrés H. Thomas^{*4} , Sherri A. McFarland^{*1,5} , Edyta M. Greer^{*6} and Alexander Greer^{*2,3} 

¹Department of Chemistry, Acadia University, Wolfville, NS, Canada

²Department of Chemistry, Brooklyn College of the City University of New York, Brooklyn, NY

³Ph.D. Program in Chemistry, The Graduate Center of the City University of New York, New York, NY

⁴INIFTA, Departamento de Química, Facultad de Ciencias Exactas, Universidad Nacional de La Plata, CCT La Plata-CONICET, La Plata, Argentina

⁵Department of Chemistry and Biochemistry, University of North Carolina at Greensboro, Greensboro, NC

⁶Department of Natural Sciences, Baruch College of the City University of New York, New York, NY

Received 17 June 2018, accepted 6 August 2018, DOI: 10.1111/php.13000

ABSTRACT

There is a major need for light-activated materials for the release of sensitizers and drugs. Considering the success of chiral columns for the separation of enantiomer drugs, we synthesized an S,S-chiral linker system covalently attached to silica with a sensitizer ethene near the silica surface. First, the silica surface was modified to be aromatic rich, by replacing 70% of the surface groups with (3-phenoxypropyl)silane. We then synthesized a 3-component conjugate [chlorin sensitizer, S,S-chiral cyclohexane and ethene building blocks] in 5 steps with a 13% yield, and covalently bound the conjugate to the (3-phenoxypropyl)silane-coated silica surface. We hypothesized that the chiral linker would increase exposure of the ethene site for enhanced ¹O₂-based sensitizer release. However, the chiral linker caused the sensitizer conjugate to adopt a U shape due to favored 1,2-diaxial substituent orientation; resulting in a reduced efficiency of surface loading; further accentuating the U shape was π - π stacking between the (3-phenoxypropyl)silane and sensitizer. Semiempirical calculations and singlet oxygen luminescence data provided deeper insight into the sensitizer's orientation and release. This study has led to insight on modifications of surfaces for drug photorelease and can help lead to the development of miniaturized photodynamic devices.

INTRODUCTION

Photoreleased molecules are of considerable interest not only in the field of photochemistry but also in site-specific delivery applications (1–23). Current literature on sensitizer and drug photorelease has mainly focused on the use of direct UV, visible and near-IR light to activate the release mechanisms. However, a utility can be exploited with photogenerated ¹O₂ (¹ Δ_g) as the

drug release trigger agent, rather than light as a direct release trigger (24–32). Although ¹O₂-release reactions are becoming common, there is a need for heterogeneous surfaces in this context to improve the selectivity of the process.

Heterogeneous surfaces have been used for photorelease reactions in the past (33–39). However, this line of research is still in its infancy. Surface types that have been studied for drug photorelease include chitosan particles (40), fluorinated silica (41), quantum dots (QDs) (42), carbon and polymer dots (43–45) and gold nanoparticles (46,47). To our knowledge, chiral surfaces that add control features to photorelease reactions have not been studied.

By contrast, many papers have been published reporting on chiral surfaces for the chromatographic separation of enantiomers. Chiral compounds such as (–)-menthyl have been covalently bonded to silica and shown to be useful as media for the separation of enantiomers (48–52). Notably, there have been some chiral surface modifications adapted for drug release. For example, porous chiral materials have been used to tune the release kinetics of R- vs S-enantiomers (53). In another example, the antitumor drug doxorubicin was released in a tunable, pH-dependent fashion to MCF-7 cells from chiral 3-N-aminopropyl-L-tartaric acid triethoxysilane porous silica particles (54).

Due to the need for the further advancement of solid supports for the photorelease of sensitizers and drugs, we sought to attach a photocleavable ethene linker to a sensitizer and introduce a bend using a chiral S,S-cyclohexyl dicarboxylate group. This required the assembly of a conjugate containing three types of monomer units: a sensitizer, a chiral cyclohexyl ring and an ethene. This trimer was then attached to 3-iodopropyl trimethoxysilane enabling the 3-component conjugate to be covalently attached to a silica surface and the sensitizer's photorelease from the silica surface to be studied, for possible PDT applications. Our detailed approach is shown in Fig. 1.

In this study, we report on the synthesis and testing of a bent [(1S,2S)-cyclohexane-1,2-dicarboxylate group] ethene linker covalently bound to silica as a unique system for the photorelease of a sensitizer. We hypothesized that the U shape of the bridge would increase the exposure of the ethene site for enhanced ¹O₂-based sensitizer release. We expected this system to be an improvement

*Corresponding authors' e-mails: athomas@inifta.unlp.edu.ar (Andrés H. Thomas); samcfarl@uncg.edu (Sherri A. McFarland); edyta.greer@baruch.cuny.edu (Edyta M. Greer); agreer@brooklyn.cuny.edu (Alexander Greer)

[†]This article is part of a Special Issue celebrating Photochemistry and Photobiology's 55th Anniversary.

© 2018 The American Society of Photobiology

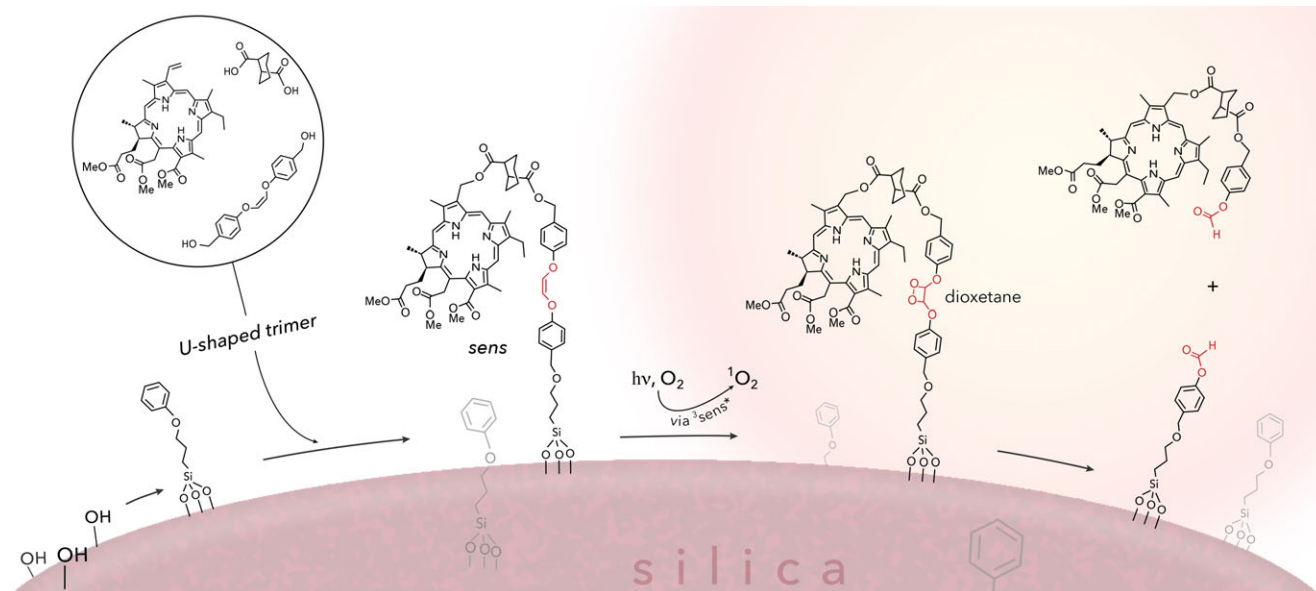


Figure 1. Illustration of the synthesis and cleavage processes: functionalization of silica with phenoxypropylsilane; the covalent attachment of the trimer conjugate drawn in a U-shaped relationship to the surface; the subsequent photorelease of the sensitizer from the silica surface. Energy transfer takes place between the triplet-state chlorin and ground-state molecular oxygen ($^3\text{O}_2$), to yield the ground state of the sensitizer and $^1\text{O}_2$. The $^1\text{O}_2$ reacts with the ethene to produce a surface-bound dioxetane, which releases the sensitizer from the surface.

over our previous succinate (55) and dimethylene-linked (56–58) sensitizer photorelease systems. In this system, the $^1\text{O}_2$, which triggers the sensitizer release, is generated by the sensitizer surface. The rapid reaction between $^1\text{O}_2$ and the ethene linker, that is, (Z)-1,2-dioxyethene, releases sensitizer molecules upon cleavage of a dioxetane intermediate (55–58). We also hypothesized that the sensitizer would be made to bend over by π - π stacking interactions with covalently bound (3-phenoxypropyl)silanes close to the surface. It was thought that our surface modification strategy would further reveal how sensitizer photorelease can be controlled, which also connects to how these materials can be engineered for miniaturized photodynamic devices.

MATERIALS AND METHODS

General information. Reagents and solvents such as methanol, hexane, toluene, *N,N*-dimethylformamide (DMF), tetrahydrofuran (THF), dichloromethane (CH_2Cl_2), chloroform (CHCl_3), deuterated chloroform (CDCl_3), carbon tetrachloride (CCl_4), *n*-butanol, sodium sulfate, sodium bicarbonate, sodium periodate, sodium borohydride, phenol, osmium tetroxide, acetic acid, *N*-(3-dimethylaminopropyl)-*N'*-ethylcarbodiimide hydrochloride (EDC), *N,N*-dimethyl-4-aminopyridine (DMAP), 3-iodopropyl trimethoxysilane and trimethylsilyl diazomethane were purchased from Sigma-Aldrich. Chlorin e_6 was purchased from Frontier Scientific. The (1*S*,2*S*)-cyclohexane-1,2-dicarboxylic acid was purchased from VWR. All the reagents and solvent were used as received from commercial suppliers without further purification. Corning 7930 porous Vycor glass (PVG) was purchased from Advanced Glass and Ceramics, Holden, MA. Silica samples were cleaned with refluxing methanol in a Soxhlet extractor. ^1H NMR spectra were collected using a Bruker Avance instrument for ^1H at 400 MHz and for ^{13}C at 100.6 MHz. UV–vis spectra were collected on a Varian Cary-100 spectrophotometer. HPLC data were obtained on a PerkinElmer 200 series instrument equipped with a bondclone 10 C18 column. HRMS data were collected at the mass spectrometry facility in University of California, Riverside. Prior to covalent attachment, PVG particles were dried using a muffle furnace (Fischer Scientific Isotemp.) for 24 h.

Synthesis of chlorin- e_6 trimethyl ester 1. Yield 100.0 mg (93.4%). To a 10-mL mixed solution (6 mL MeOH and 4 mL toluene), 100.0 mg (0.167 mmol) of chlorin e_6 was added and stirred for 5 min under

nitrogen. A 460 μL (0.924 mmol) 2 M hexane solution of trimethyl silyl diazomethane was added to the reaction mixture drop wise. Reaction mixture was stirred under N_2 for 5 h. AcOH (10 mL 10% aqueous solution) was added to the reaction mixture to quench excess diazomethane. MeOH was evaporated under reduced pressure. Reaction mixture was diluted with 20 mL dichloromethane, and organic layer was washed three times with 10 mL water and dried on Na_2SO_4 and evaporated to get crude product. Crude product was separated by column chromatography using 0.2% MeOH in CH_2Cl_2 . $R_f = 0.85$. HPLC showed the purity of the compound is 99%: $t_R = 19.2$ min in gradient mixture of MeOH and H_2O . ^1H NMR (400.0 MHz, CDCl_3) δ 9.72 (s, 1H), 9.54 (s, 1H), 8.80 (s, 1H), 8.03 (dd, $J = 18.0$ Hz, 11.6 Hz, 1H), 6.34 (d, $J = 18.0$ Hz, 1H), 6.13 (d, $J = 11.2$ Hz, 1H), 5.44 (d, $J = 18.8$ Hz, 1H), 5.33 (d, $J = 13.6$ Hz, 1H), 4.51 (m, 2H), 4.33 (s, 3H), 3.84 (s, 3H), 3.77 (m, 2H), 3.70 (s, 3H), 3.64 (s, 3H), 3.48 (s, 3H), 3.29 (s, 3H), 2.63 (m, 1H), 2.26 (m, 2H), 1.83 (d, $J = 7.6$ Hz, 4H), 1.75 (t, $J = 11.2$ Hz, 3H), –1.22 (br s, 1H), –1.37 (br s, 1H).

Synthesis of 3-formyl chlorin e_6 trimethyl ester 2. Yield 52.0 mg (56%). To the 90.0 mg (0.141 mmol) of **1** in 25 mL THF, 15.36 mg (0.06 mmol) of OsO_4 in 150 μL CCl_4 was added at 0°C under N_2 atmosphere. Reaction mixture was stirred within 0 – 5°C temperature for 25 min. A known value of 254 mg (1.19 mmol) of NaIO_4 , dissolved in 5% AcOH solution, was added to the reaction mixture. Reaction mixture was stirred overnight at room temperature. THF was evaporated out in rotavapor. Reaction mixture was extracted with 50 mL of dichloromethane and washed with water. The organic layer was dried over sodium sulfate. After evaporating organic solvent, residue was purified by column chromatography using 0.1% MeOH- CH_2Cl_2 . $R_f = 0.62$ in 1% MeOH- CH_2Cl_2 . ^1H NMR (400.0 MHz, CDCl_3) δ 11.52 (s, 1H), 10.23 (s, 1H), 9.67 (s, 1H), 8.97 (s, 1H), 5.43 (d, $J = 19.2$ Hz, 1H), 5.31 (d, $J = 18.8$, 1H), 4.51 (m, 2H), 4.31 (s, 3H), 3.82 (s, 3H), 3.80 (s, 3H), 3.69 (s, 3H), 3.61 (s, 3H), 3.30 (s, 3H), 2.66 (m, 1H), 2.30 (m, 2H), 2.19 (m, 4H), 1.79 (m, 3H), 1.72 (t, $J = 7.6$, 4H), –1.77 (br s, 1H); ^{13}C NMR (100.6 MHz, CDCl_3) δ 188.3, 173.5, 172.8, 169.1, 168.9, 167.5, 155.1, 151.6, 145.0, 138.3, 138.2, 138.0, 136.5, 136.0, 134.0, 131.9, 128.5, 125.5, 103.2, 101.3, 100.7, 95.6, 53.5, 53.2, 52.2, 51.7, 48.7, 38.5, 31.0, 29.7, 29.3, 23.2, 19.6, 17.6, 12.4, 11.4, 11.3.

Synthesis of 3'-hydroxyl chlorin- e_6 trimethyl ester 3. Yield 39.3 mg (98%). To the 10 mL MeOH- CH_2Cl_2 (4:1 mixture), 40.0 mg (0.062 mmol) of **2** and 9.0 mg (0.23 mmol) of NaBH_4 was added in ice-cold temperature. Color of the solution was changed from red to emerald green. Reaction was stirred in room temperature for 15 h. MeOH was evaporated by reduced pressure. Reaction mixture was diluted with

25 mL CH_2Cl_2 . Organic layer was washed with 10 mL 5% AcOH followed by saturated sodium bicarbonate and water. Organic layer was dried on Na_2SO_4 and evaporated on rotavapor to get green solid. Crude product showed single spot in TLC. Therefore, column chromatography was not performed. $R_f = 0.32$ in 1% MeOH- CH_2Cl_2 . ^1H NMR (400.0 MHz, CDCl_3) δ 9.69 (s, 1H), 9.52 (s, 1H), 8.77 (s, 1H), 5.83 (s, 2H), 5.38 (d, $J = 19.2$, 1H), 5.30 (d, $J = 11.2$, 1H), 4.46 (m, 2H), 4.28 (s, 3H), 3.80 (s, 3H), 3.65 (s, 3H), 3.60 (s, 3H), 3.43 (s, 3H), 3.27 (s, 3H), 2.59 (m, 1H), 2.21 (m, 3H), 1.78 (d, $J = 7.2$, 4H), 1.71 (t, $J = 7.6$, 4H), -1.61 (br s, 1H); ^{13}C NMR (100.6 MHz, CDCl_3) δ 173.6, 173.0, 169.6, 169.4, 167.0, 154.3, 148.7, 145.0, 139.1, 136.7, 136.0, 135.6, 135.4, 135.1, 132.6, 129.4, 123.5, 102.4, 102.0, 98.2, 93.8, 56.3, 53.1, 53.0, 52.1, 51.7, 49.3, 38.6, 31.0, 29.7, 29.5, 22.9, 19.6, 17.6, 12.4, 11.3, 11.1.

Synthesis of trans-cyclohexyl monocarboxylate chlorin e_6 trimethyl ester 4. Yield 30.0 (60%). To the 40.0 mg (0.062 mmol) of **3** in 10 mL of dry dichloromethane under nitrogen atmosphere, 42.8 mg (0.24 mmol) of (1*S*,2*S*)-cyclohexane-1,2-dicarboxylic acid, 23.79 mg (0.12 mmol) of EDC and 15.07 mg (0.12 mmol) of DMAP was added. Reaction mixture was stirred for 24 h under N_2 in room temperature. CH_2Cl_2 was evaporated and compound was purified by column chromatography using 1–1.2% MeOH- CH_2Cl_2 . $R_f = 0.33$ in 1.5% MeOH- CH_2Cl_2 . HPLC showed the purity of the compound is 87%: $t_R = 16.0$ min in gradient mixture of MeOH and H_2O . ^1H NMR (400.0 MHz, CDCl_3) δ 9.70 (s, 1H), 9.56 (s, 1H), 8.80 (s, 1H), 6.49 (d, $J = 12.8$, 1H), 6.31 (d, $J = 12.8$, 1H), 5.38 (d, $J = 18.8$, 1H), 5.26 (d, $J = 18.8$, 1H), 4.45 (m, 2H), 4.28 (s, 3H), 3.79 (s, 3H), 3.64 (s, 3H), 3.58 (s, 3H), 3.48 (s, 3H), 3.32 (s, 3H), 2.72 (m, 2H), 2.55 (m, 1H), 2.19 (m, 2H), 2.04 (m, 2H), 1.76 (d, $J = 7.2$, 3H), 1.69 (m, 6H), 1.23 (m, 8H), -1.64 (brs, 1H).

Synthesis of spacer (Z)-2-phenoxyvinylbenzyl-(1*S*,2*S*)-cyclohexane-1,2-dicarboxylate chlorin- e_6 trimethyl ester 5. Yield 17.7 mg (42%). To the 30.0 mg (0.04 mmol) of **4** in 10 mL of dry dichloromethane in nitrogen atmosphere, 30 mg (0.12 mmol) of spacer alkene alcohol, 15.3 mg (0.08 mmol) of EDC and 9.7 mg (0.08 mmol) of DMAP was added. Reaction mixture was stirred for 24 h under N_2 in room temperature. CH_2Cl_2 was evaporated, and compound was purified by column chromatography using 0.35–0.45% MeOH- CH_2Cl_2 . $R_f = 0.51$ in 1.5% MeOH- CH_2Cl_2 . HPLC showed the purity of the compound is 95%: $t_R = 18.5$ min in gradient mixture of MeOH and H_2O . ^1H NMR (400.0 MHz, CDCl_3) δ 9.74 (s, 1H), 9.58 (s, 1H), 8.80 (s, 1H), 7.21 (d, $J = 8.4$ Hz, 2H), 6.90 (d, $J = 8.4$ Hz, 2H), 6.80 (d, $J = 8.4$ Hz, 2H), 6.54 (d, $J = 8.4$ Hz, 2H), 6.46 (d, $J = 12.8$ Hz, 1H), 6.31 (d, $J = 12.8$ Hz, 1H), 5.80 (d, $J = 3.6$ Hz, 1H), 5.53 (d, $J = 3.2$ Hz, 1H), 5.39 (d, $J = 19.2$ Hz, 1H), 5.27 (d, $J = 18.8$ Hz, 1H), 4.79 (d, $J = 12.0$ Hz, 1H), 4.65 (d, $J = 12.0$ Hz, 1H), 4.55 (brs, 2H), 4.46 (m, 2H), 4.29 (s, 3H), 3.82 (m, 6H), 3.67 (s, 3H), 3.61 (s, 3H), 3.48 (s, 3H), 3.34 (s, 3H), 2.78 (m, 2H), 2.60 (m, 1H), 2.15 (m, 4H), 1.75 (m, 10H), 1.39 (m, 2H), 1.28 (m, 3H), -1.48 (brs, 1H), -1.79 (brs, 1H); ^{13}C NMR (100.6 MHz, CDCl_3) δ 175.0, 174.7, 173.7, 173.6, 173.4, 173.0, 169.4, 167.1, 156.8, 156.7, 154.7, 149.3, 145.1, 138.7, 136.6, 136.3, 135.4, 135.3, 134.0, 131.1, 129.9, 129.6, 129.3, 128.4, 128.2, 127.6, 123.7, 116.0, 115.6, 115.5, 115.4, 102.4, 102.0, 98.5, 94.0, 65.6, 64.7, 57.4, 53.1, 53.0, 52.1, 51.6, 49.3, 45.1, 45.0, 42.8, 42.7, 38.5, 31.1, 29.7, 29.5, 29.0, 28.9, 25.1, 22.9, 19.6, 17.7, 12.4, 11.3, 11.2. (+ESI) m/z calculated for $\text{C}_{60}\text{H}_{67}\text{N}_4\text{O}_{13}$ $[\text{M}+\text{H}]^+$ 1051.4699, found: 1051.4716.

Covalent binding of conjugate 5 and phenoxypropylsilane to silica. Phenoxypropylsilane was attached to silica following the methodology of nonafluorosilane $[(\text{CH}_3\text{O})_3\text{SiCH}_2\text{CH}_2\text{CF}_2\text{CF}_2\text{CF}_2\text{CF}_3]$ attachment to silica

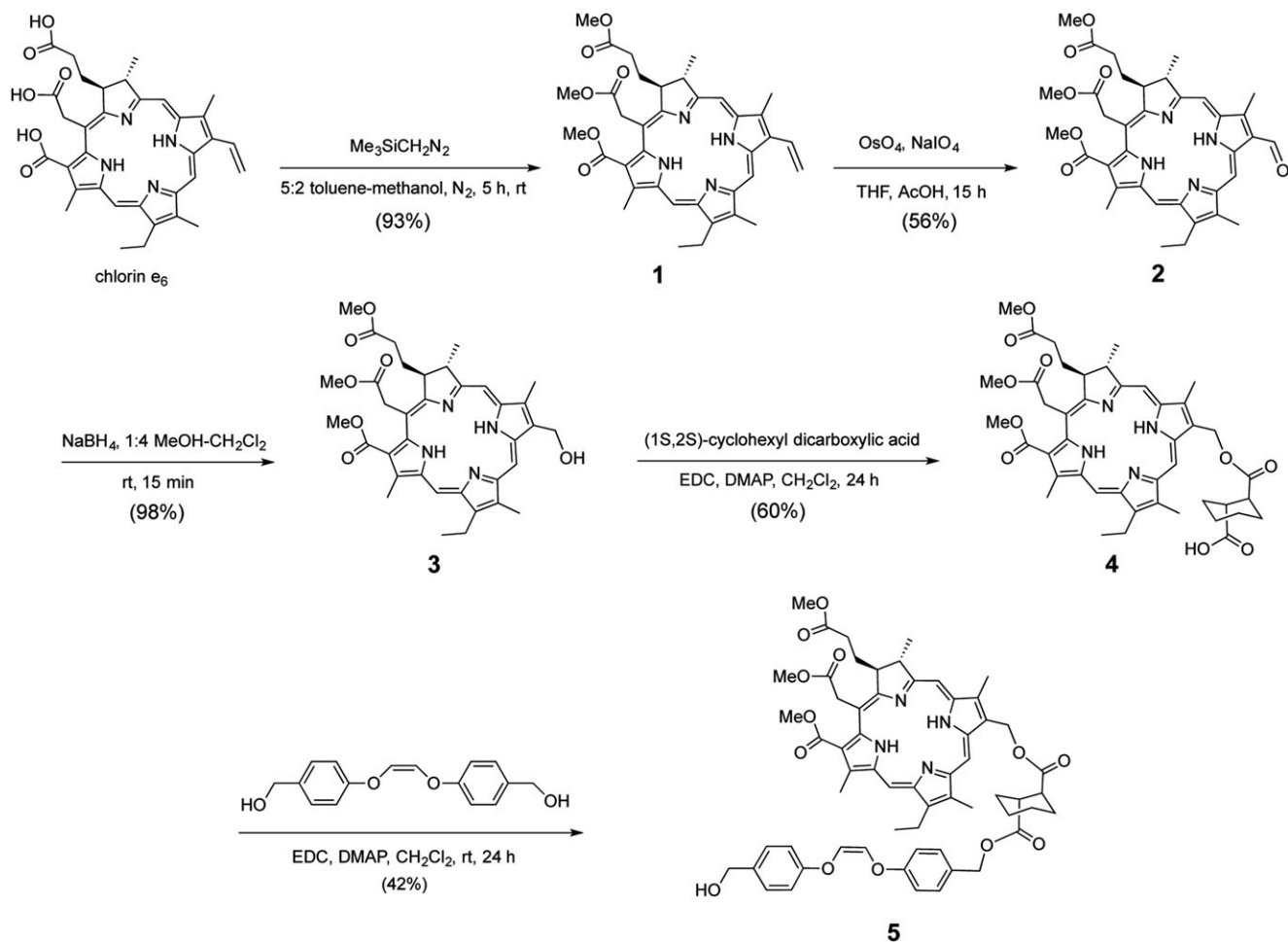


Figure 2. Synthesis of conjugate **5** from three building blocks: a chlorin sensitizer, a (1*S*,2*S*)-cyclohexane, and an ethene [i.e. a (Z)-(ethene-bisphenylene)dimethanol].

(41). 3-Iodopropyl trimethoxysilane (0.783 g, 2.62 mmol) and NaH (94.3 mg, 3.93 mmol) were added to 0.244 g (2.62 mmol) of phenol in 50 mL of dry THF. Mixture was refluxed at 70°C for 24 h. THF was evaporated completely after the reaction, and 1.0 g of silica was added *in situ* and refluxed in toluene for another 24 h. Silica particles were separated by filtration and washed with CH₂Cl₂, THF, methanol, toluene and hexane and then Soxhlet extracted with methanol for 24 h to get phenol conjugated silica particle **6**. Then, 5 mg (4.75 μmol) of **5** reacted with 3-iodopropyl trimethoxysilane in THF in a round bottom flask. THF was completely evaporated and phenol conjugated silica particle to that flask and toluene were added and refluxed for 24 h to get chlorin trimethyl ester conjugated phenolic silica particle **7**. It was then washed with CH₂Cl₂, THF, methanol and hexane followed by its Soxhlet extraction in methanol for 24 h to remove any adsorbed sensitizer from the silica. No sensitizer leaching from the surface was observed in the dark. Silica was dissolved by HF treatment and suspended green solid in the aqueous solution was extracted with CHCl₃, evidence suggested the liberation of sensitizer as characteristic Soret and Q-band was found at 400 and 660 nm, respectively, in UV-vis of CHCl₃.

Quantifying the loading of conjugate 5 on silica. Sensitizer loading on **7** was calculated by the HF stripping method. A known value of 100.0 mg of sensitizer modified silica **7** was placed in 2.0 mL 50% (v/v) HF solution and kept 3.0 h in room temperature. Sensitizer was extracted

from aqueous HF solution by CHCl₃. The concentration of sensitizer in CHCl₃ was calculated based on a calibration plot of **5** by monitoring the Soret absorption band (400 nm). Sensitizer loaded on silica **7** is 378 nmol g⁻¹.

Singlet oxygen measurements. Time-resolved experiments were performed at room temperature using a near-IR PMT Module H10330-45 (Hamamatsu, Iwata City, Japan) coupled to FL3 TCSPC-SP (Horiba Jobin Yvon) single-photon-counting equipment, as described elsewhere (59). Steady-state experiments were conducted with samples in a quartz cell irradiated with a CW 450W Xe source equipped with an excitation monochromator. The luminescence, after passing through an emission monochromator, was detected at 90° with respect to the incident beam using a near-IR photomultiplier tube. Emission spectra were recorded between 950 and 1400 nm. For some steady-state experiments, a CW diode laser with an output of 669 nm was used. The singlet oxygen quantum yield (Φ_{Δ}) of silica **7** was not determined due to complicating factors including: light scattering of the particles; small ¹O₂ emission signal prior to sensitizer cleavage away from the particle; and interference from the spacer ethene that acts as a ¹O₂ chemical quencher.

Computational details. Semiempirical PM6 method (60) available in Gaussian 09 program package with revision D.01 (61) was used to generate scans by rotating dihedral angle Φ (C1-O2-C3-C4) and dihedral angle θ (C1'-O2'-C3'-C4') by 360° in increments of 60°. The

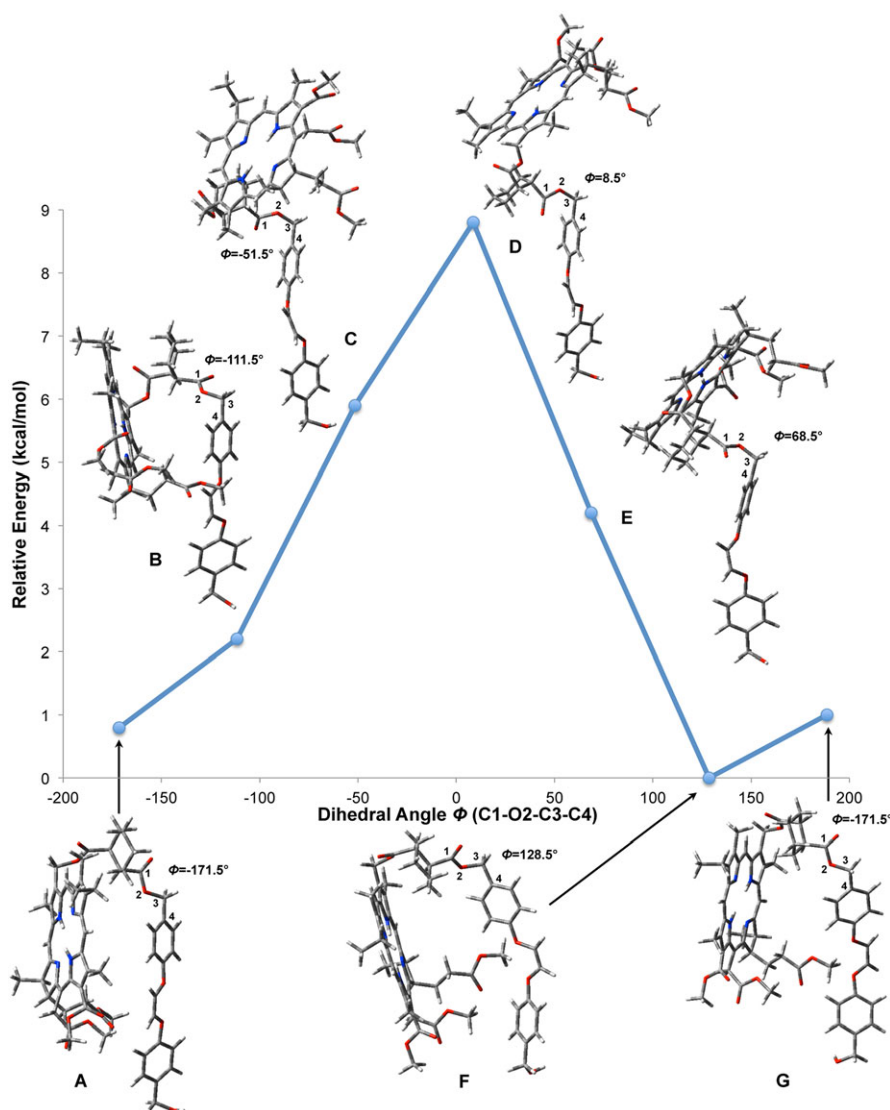


Figure 3. PM6 computed energies of various conformations of conjugate **5** by rotation of a dihedral angle Φ (C1-O2-C3-C4) by 360° in increments of 60°. The dihedral angle C1-O2-C3-C4 is defined as negative in a counter-clockwise direction down the O2-C3 bond. Low energy conformers **A**, **B**, **F** and **G** show a *syn* orientation (U shape) of the sensitizer and ethene groups. Conformer **F** was the lowest energy minimum found.

PM6 method was selected was used successfully for modeling large systems, namely proteins, where protein structures optimized with PM6 reproduced experimental X-ray structures (62). The GaussView 5.0 program was used for visualization of the molecules (63).

RESULTS AND DISCUSSION

Our approach was to synthetically load the sensitizer conjugate onto silica and to analyze conformations and photorelease of the sensitizer from the silica surface.

Synthesis and characterization of compounds 1-5

The sensitizer-cyclohexyl-ethene trimer **5** was synthesized in five steps from chlorin e_6 with 13% overall yield (Fig. 2).

Step 1: Chlorin e_6 was reacted with trimethylsilyl diazomethane to reach chlorin e_6 -trimethyl ester **1** in 93% yield using a modified procedure from the literature, where

diazomethane gas was used for the conversion. Compound **1** produced six distinct singlets for six methyl groups (three from methyl esters and the other three from pyrrole moiety) by ^1H NMR. Compound **1** is known in the literature (64).

Step 2: Compound **1** was then reacted with OsO_4 followed by a 10% acetic acid solution of NaIO_4 to yield 3-formyl chlorin e_6 -trimethyl ester **2** with 56% yield using a procedure of Shim *et al.* (65). ^1H NMR showed four singlets (11.52, 10.23, 9.67 and 8.97 ppm), with the peak at 11.52 ppm assigned to the aldehyde and the others to the *meso* hydrogens, which indicate the conversion of the 3^1 - 3^2 vinyl bond to 3-formyl.

Step 3: NaBH_4 reduction in the 3-formyl to its corresponding alcohol gave 3¹-hydroxyl chlorin e_6 -trimethyl ester **3** in 98% yield based on the procedure of Pavlov *et al.* (66). Formation of **3** was evidenced by proton NMR, where

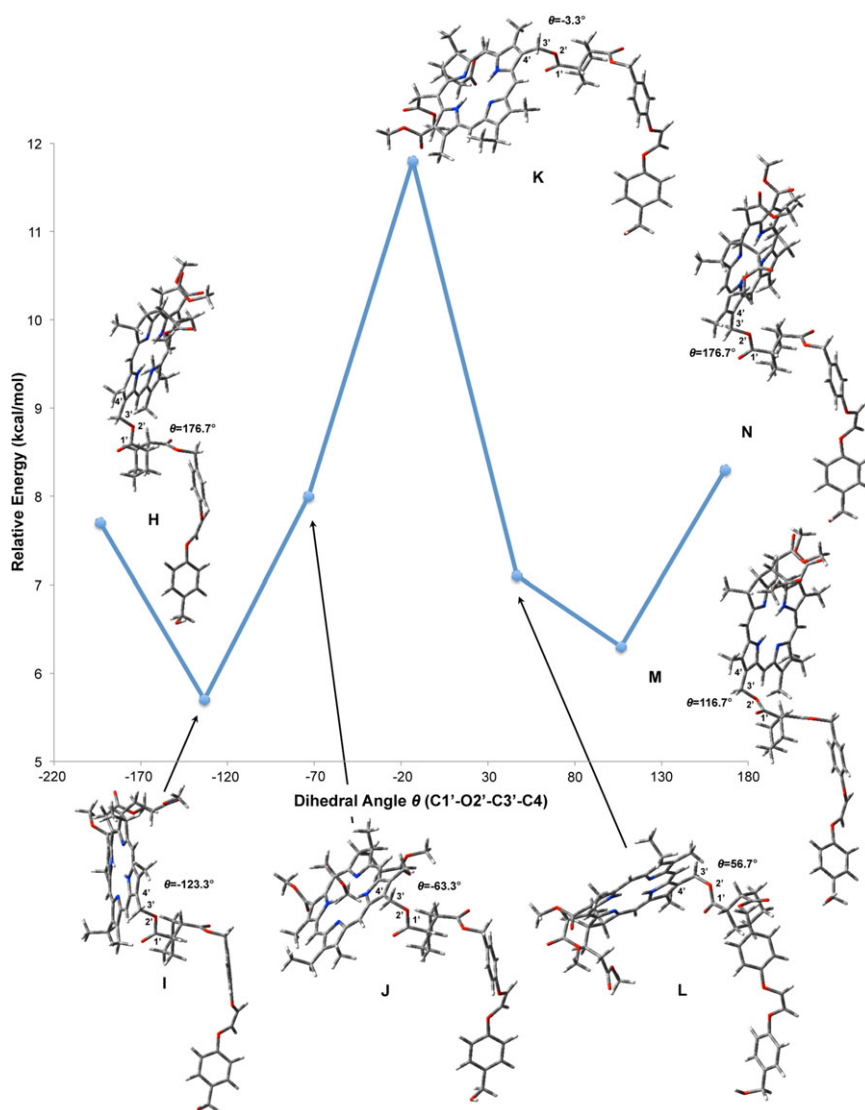


Figure 4. PM6 computed energies of various conformations of conjugate **5** by rotation of a dihedral angle θ ($\text{C1}'\text{-O2}'\text{-C3}'\text{-C4}'$) by 360° in increments of 60° . The dihedral angle $\text{C1}'\text{-O2}'\text{-C3}'\text{-C4}'$ is defined as negative in a counter-clockwise direction down the $\text{O2}'\text{-C3}'$ bond. Conformers show a U- or L-bend or straight relationship between the sensitizer and ethene groups. Energies are relative to conformer **F** in Fig. 3, which was the lowest energy minimum found.

the aldehyde peak at 11.52 ppm for **2** was absent in the spectrum of **3**.

Step 4: (1*S*,2*S*)-cyclohexane-1,2-dicarboxylic acid was coupled to **3** using EDC-DMAP, a common coupling reagent for esterification reactions (58,67), to afford monoester **4** in 60% yield. Esterification of the 3¹-hydroxyl group resulted in a downfield shift of the two protons attached to 3¹-carbon. Each of these two protons appeared as two distinct doublets at 6.49 and 6.31 ppm with $J = 12.8$ Hz. The splitting of these hydrogens into doublets suggests that attachment of the cyclohexane moiety produces a different electronic environment for each proton.

Step 5: The (*Z*)-(ethene-bisphenylene)dimethanol was coupled to **4** using EDC-DMAP to afford the 3-component conjugate **5** in 42% yield. (The (*Z*)-(ethene-bisphenylene) dimethanol was synthesized in 5 steps following a literature procedure) (58). The ¹H NMR spectrum of trimer **5** exhibited eight phenyl protons (7.21, 6.90, 6.80 and 6.54 ppm, $J = 8.4$ Hz). The alkene hydrogens gave rise to a doublet at 5.80 and 5.54 ppm. 2D HSQC indicated that the four doublets produced by the phenyl hydrogens correlated to carbon signals at 129.3, 128.4, 116.0 and 115.4 ppm and that the two alkene doublets correlated to the carbons at 128.2 and 127.6 ppm (Figure S9). Following the synthesis

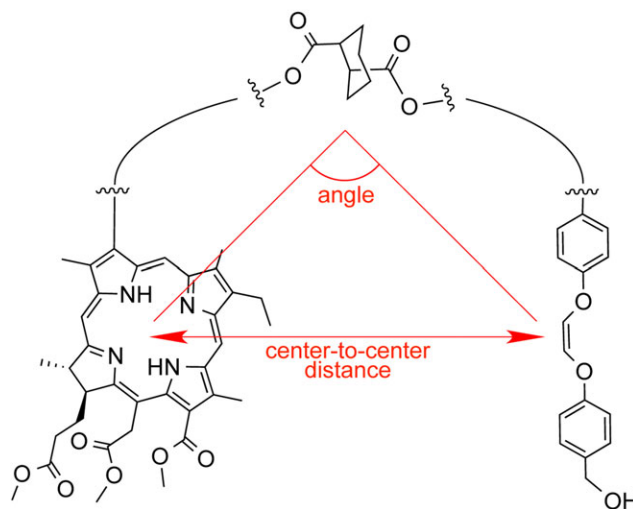
of trimer **5**, semi-empirical PM6 calculations were performed, in order to gain insight on the preferred orientation of the sensitizer relative to the ethene group. These calculations are described next.

Computed conformations show a bent-shaped three-component conjugate **5**

In order to explore the conformations of trimer **5** connecting sensitizer, *trans*-cyclohexyl, and ethene together, PM6 calculations were carried out. In various conformations, trimer **5** was found to fold into a U- or L-shape in order to reach its energetically preferred structure. When straightened geometries were sought, the energy increased, where optimized structures were mainly bent structures. The conformers in Figs. 3 and 4 show 14 optimized conformations of trimer **5**. Conformer **F** was the most stable. Conformers **A-E** and **G-N** were found to be within 12 kcal mol⁻¹ by C1–O2–C3–C4 bond rotations about the (1*S*)-cyclohexane group and C1'–O2'–C3'–C4' bond rotations about the (2*S*)-cyclohexane group. Thus, the conformers are flexible and are expected to exist as a mixture in solution.

Table 1 shows the through-space distance from the center of the sensitizer to the center of the ethene C=C bond in conformers **A-N** ranges from 7.7 Å to 14.9 Å. Table 1 also

Table 1. PM6 computed distances from the center of the sensitizer and ethene sites in conformers **A-N**.



Conformer	Distance (Å)	Angle (°)	Shape
A	7.7	49.9	U
B	7.9	53.2	U
C	12.1	95.9	L
D	14.0	131.8	L
E	12.6	119.8	L
F	9.7	65.3	U
G	10.1	66.1	U
H	14.7	132.7	Straight
I	14.4	160.4	L
J	13.5	133.4	L
K	13.9	118.0	L
L	13.2	109.9	L
M	14.7	136.2	Straight
N	14.9	142.0	Straight

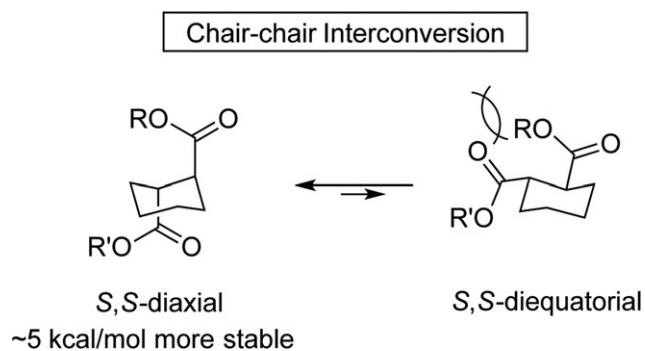


Figure 5. The *S,S*-diaxial orientation is preferred over the *S,S*-diequatorial orientation.

shows the shapes of conformers due to the intervening chiral *S,S*-cyclohexyl group based on PM6 computations. Furthermore, the calculations show a clear preference for a U shape in trimer **5**, where the conformer **F** contains a 65° angle (center of the sensitizer—center of the cyclohexyl—center of the ethene). The *S,S*-cyclohexyl group serves as the arced bend of the U structure. The U shape is based on a favored diaxial rather than diequatorial substituent orientation as shown in Fig. 5. In contrast, previously reported sensitizer–ethene dimers (55–58) contain no such bending group and are thought to adopt linear conformations due to their dimethylene or succinate connecting groups.

The U shape of trimer **5** somewhat resembled structures found in the literature (68–72), such as the bent-shaped conformers in kibdelymycin bound to *S. aureus* (73), or the aminomalonyl dipeptide esters (74) and fluorescent naphthalimide-cholesterol conjugates in membranes (75). Next, the U shape of the sensitizer conjugate was examined with regard to the surface loading and $^1\text{O}_2$ -based ethene cleavage relative to that reported in the literature. The former effect is described next.

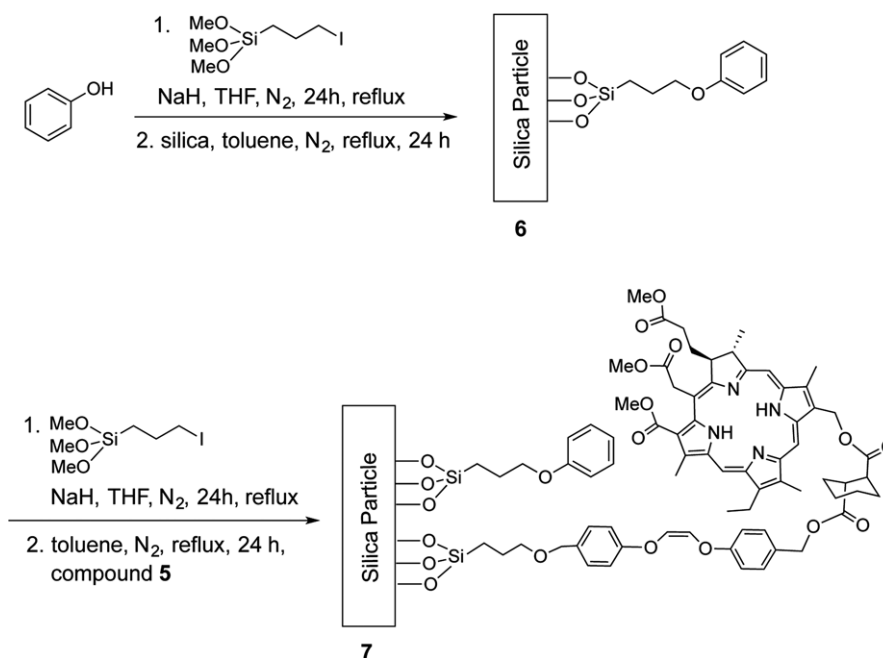


Figure 6. Synthesis of phenoxypropyl silica particle **6** and the sensitizer conjugated phenoxypropyl silica particle **7**.

Covalent bonding of trimer conjugate to a phenoxypropyl-coated silica surface

Fine particles of diameters ranging from 75 to 150 μm were prepared by grinding and sieving porous Vycor glass (PVG) according to our previously reported method (57). Next, phenol molecules were covalently attached to the silica surface by a reaction with 3-iodopropyl trimethoxysilane as seen in Fig. 6. In our reaction, phenoxypropyl trimethoxysilane $(\text{MeO})_3\text{SiCH}_2\text{CH}_2\text{CH}_2\text{OPh}$ was formed *in situ* and bound with silica. The reaction resulted in coverage of 70% of the silica surface (1.16 mmol g^{-1} silica) with OPh groups. The use of 3-iodopropyl trimethoxysilane to covalently attach compound on a silica surface had been previously successful (76–78). Sensitizer-coated surface **7** was then synthesized by reacting trimer **5** with 3-iodopropyl trimethoxysilane and attaching it to the (3-phenoxypropyl)silane coated silica surface by some of the remaining silanol groups. Soxhlet extraction was used to remove any noncovalently bound compounds. The trimer's silica surface coverage was determined by obtaining UV-vis of the sensitizer liberated by dissolving the silica **7** in aqueous HF, by a method previously reported (41,55,79,80). Based on the data gained through this HF treatment, the coverage of sensitizer molecules in **7** was found to be 0.023% (0.38 $\mu\text{mol g}^{-1}$ silica).

As noted in the computational studies reported above, the U shape of trimer **5** may discourage it from bonding to the silica surface by hindering the silane portion of **5** from reaching the surface. Our results for the U shape orientation between the sensitizer and ethene suggest the sensitizer would be directed toward the surface. This conformation could potentially impact the photorelease chemistry, which we investigated next.

Singlet oxygen induced release of sensitizer **9** from the silica **7**

Silica **7** was investigated by direct analysis of the $^1\text{O}_2$ near-IR luminescence (81,82) (Fig. 7). Silica **7** was stirred and irradiated

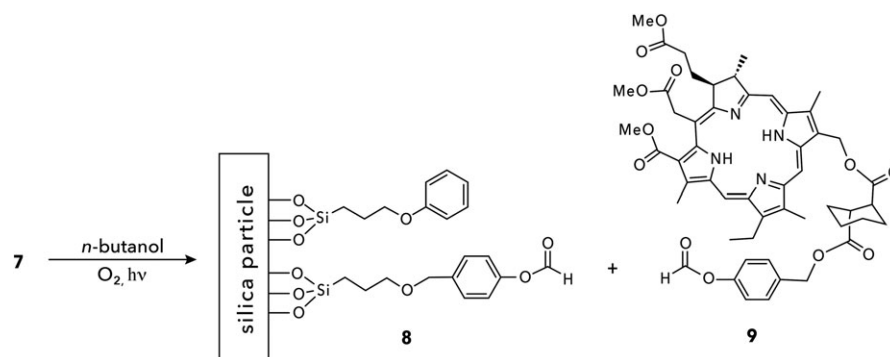


Figure 7. The photooxidation of sensitizer conjugated phenoxypropyl surface **7** leads to the release of sensitizer **9**. The released sensitizer **9** is nonrigid but may retain a U shape based on the conformational scans shown in Figs. 3 and 4.

simultaneously, while the near-IR emission spectra were recorded after the sample was excited at the wavelengths of the Soret (400 nm) and the Q-band (660 nm) of the sensitizer. The typical $^1\text{O}_2$ phosphorescence band centered at 1270 nm was observed upon irradiation of silica **7** as seen in Fig. 8, providing clear evidence of $^1\text{O}_2$ production. Interestingly, the $^1\text{O}_2$ emission arises early in the reaction suggesting the production of singlet oxygen while the sensitizer is bound to the particle, but this is very low compared to when the sensitizer is photoreleased into solution. That is, the intensity of the $^1\text{O}_2$ phosphorescence increased as the irradiation time increased wherein the sensitizer is released and diffused into solution.

In another set of experiments, silica **7** was irradiated at 400 nm for 2 h in chloroform and then the particles were removed from solution by centrifugation. The resulting chloroform solution (supernatant) produced $^1\text{O}_2$ upon visible-light irradiation, indicating that the sensitizer photorelease from the particles had occurred. The results suggest that $^1\text{O}_2$ reacts with the ethene and forms a dioxetane intermediate, which breaks its C–C and O–O bonds to give stable carbonyl-containing compounds. Because the total rate constant (k_T) of $^1\text{O}_2$ with dialkoxyethene is $\sim 4 \times 10^7 \text{ M}^{-1} \text{ s}^{-1}$ (83), hundreds of collisions between the two are required in this sub-diffusion controlled process that leads to sensitizer cleavage. The cleaved sensitizer **9** dissolves in solution and leads to $^1\text{O}_2$ luminescence in the solution phase. The sensitizer release is shown not to occur in the dark by a reaction such as hydrolysis.

The results shown in Table 2 (entry 1) indicate a low sensitizer photorelease efficiency of 5% after 1 h of irradiation at 669 nm, as determined by monitoring the appearance of the released sensitizer's Q-band absorption in *n*-butanol. The sensitizer photorelease efficiency increased substantially (68–99%) with a dimethylene or succinate linker (Table 2, entries 2–4) (41,55–58). A previous report (58) also showed the optimal photorelease rate was obtained with sensitizer loading of $4.4 \mu\text{mol g}^{-1}$ silica and a sensitizer-to-sensitizer distance of 17 nm (Table 2, entry 2). Due to the limited surface coverage achieved with the U-shape trimer **5**, only $0.38 \mu\text{mol g}^{-1}$ silica, the sensitizer-to-sensitizer distance of 660 nm is less than optimal (Table 2, entry 1). Nonetheless, the dialkoxyethene group reacts rapidly with $^1\text{O}_2$, similar to successful $^1\text{O}_2$ -based C=C and C=N bond types (e.g. disulfidoethenes, aminoacrylates, oximes, vinylimines and hydrazones) that also undergo cleavage as reported in the literature (84–88). Next, the mechanistic facets of the bent sensitizer conjugate were analyzed.

Mechanistic considerations

Our computed and experimental results provide insight on how the bent orientation effects covalent attachment and sensitizer photorelease (Fig. 9). We found that (1) the sensitizer-cyclohexane-ethene trimer was successfully synthesized, and PM6 computations show that it adopts a U shape. (2) The bonding of the sensitizer to the silica surface was low when a (1*S*,2*S*)-cyclohexane linker was introduced. Table 2 provides information that its loading (entry 1) is 6–33 times *lower* compared to reports that use a dimethylene or succinate linker on native silica (entry 2) and fluorinated silica (entries 3 and 4). (3) Not only does the curvature of the *S,S*-cyclohexane linkage restrict bonding of the silane to the surface, it also *restricts* the sensitizer photorelease. Sensitizer particle **7** was 14–17-times less efficient at photorelease, as can be seen in Table 2 when comparing to native silica (entry 2) and fluorinated silica samples (entries 3 and 4). (4) We surmise that sensitizer silica **7** is further influenced by π - π stacking interactions between the phenoxypropyl and chlorin sites on the surface. This

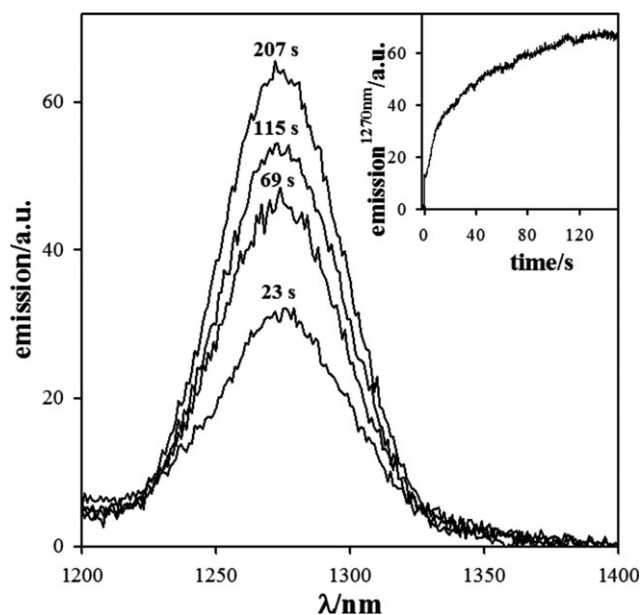
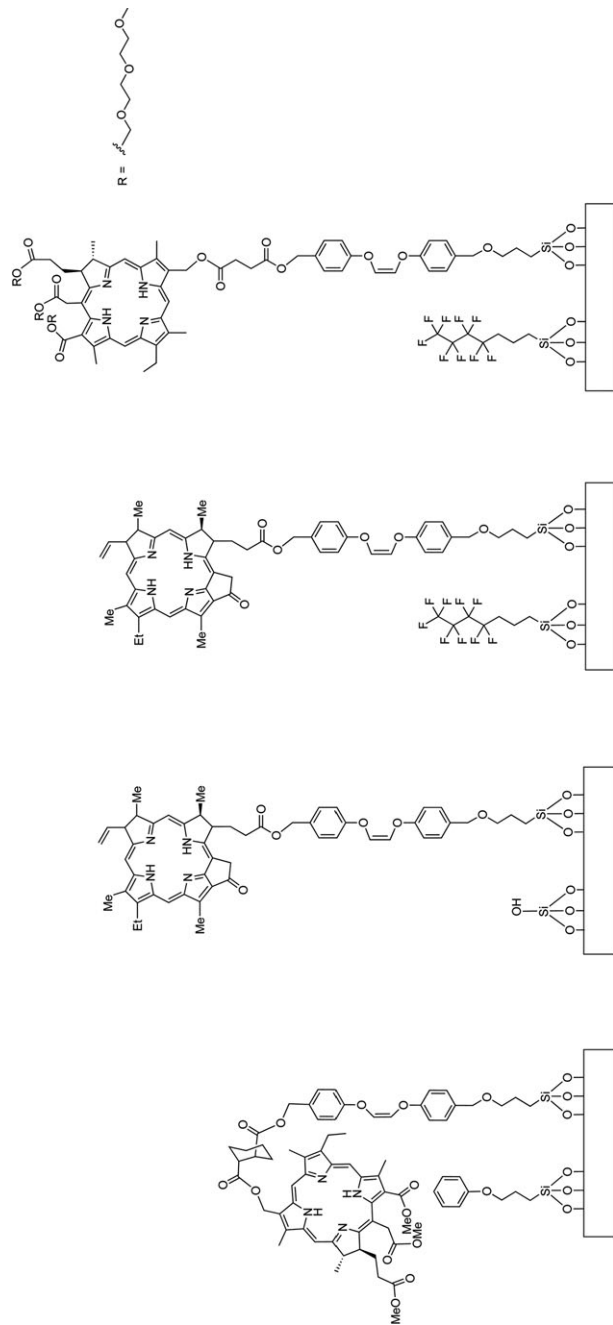


Figure 8. Near-IR emission spectra registered at different irradiation time of particles **7**. Inset: Emission at 1270 nm during irradiation of particles **7**. Excitation wavelength 400 nm.

Table 2. Information on covalent bonding to silica and photorelease.

Entry	Particle type*	Sensitizer loading ($\mu\text{mol g}^{-1}$ silica) ^y	Sensitizer loading/gram silica (%) ^z	Fluorosilane and phenoxypropyl-silane loading (mmol g^{-1} silica)	Fluorosilane and phenoxypropyl-silane loading (g^{-1} silica)	Sens:fluorosilane: SiOH and sens: phenoxypropyl-silane:SiOH	Sens: SiOH	Sens: fluorosilane: sens distance (nm)	Sens-fluorosilane and sens-OPh distance (nm)	Fluorosilane-fluorosilane distance (nm)	PhO-PhO distance (nm)	Amount of sensitizer photoreleased	Reference
1	Chlorin-(1,5,2S)-cyclohexane-ethene	0.38	0.023	1.2	70	1:1300	1:1300	660	1.2	–	1.2	2 nmol (5% in <i>n</i> -butanol)	This work
2	Phenophorbide-dimethylene-ethene native silica ¹⁰	4.4	0.26	–	–	1:380	1:380	17	–	–	–	0.25 μmol (6% in toluene- <i>d</i> ₈), 12.5 μmol (99% in octanol)	(56, 58)
3	Phenophorbide-dimethylene-ethene fluorinated silica ¹¹	11.3–12.5	0.68–0.75	1.6	96	1:5 to 1:140:5	1:130:5	12	1.0	1.0	–	11.1 μmol (89% in toluene- <i>d</i> ₈), 93% in <i>n</i> -butanol	(41, 57)
4	TriPEGchlorin-succinate-ethene fluorinated silica ¹²	2.2	0.13	1.6	96	1:30	1:740:30	28	1.0	1.0	–	1.5 μmol (68% in <i>n</i> -butanol)	(55)

*



7

10

11

12

^ySensitizer loading was calculated based on the hydrofluoric acid (HF) stripping method as described in the Experimental section. ^zPercent loading of sensitizer in fluorinated or phenoxypropyl silica was calculated based on the initial amount of silanols (Si-OH) present in the silica before covalently bonding phenoxypropyl-silane or nonafluorosilane was $1.66 \times 10^6 \text{ nmol g}^{-1}$ silica.

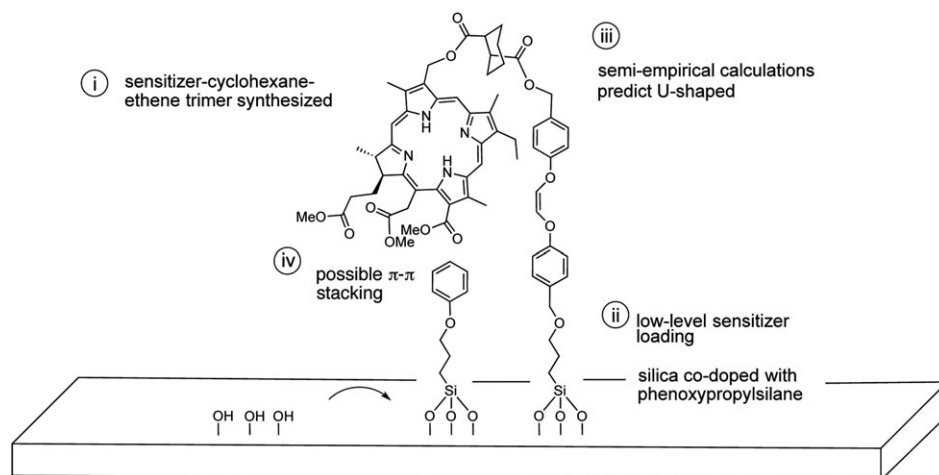


Figure 9. The proposed mechanistic outcome when the *S,S*-chiral spacer is used in conjugate synthesis, loading, conformation control and $^1\text{O}_2$ -cleavage. (1) The sensitizer-(1*S*,2*S*)-cyclohexane-ethene conjugate is synthesized, and (2) bonded to silica co-doped with phenoxypropylsilane groups. The loading of the trimer conjugate is restricted due to a U shape, that is, a *syn*-facial sensitizer and ethene group. (3) The U shape also leads to less photoreleased sensitizer in comparison with the literature dimethylene and succinate spacers thought to have an extended structure, an *anti*-situated sensitizer and photocleavable ethene groups. (4) Possible π - π stacking with phenoxypropyl groups can further accentuate the curvature of the sensitizer toward the surface.

is similar to literature reports of porphyrin dimers that intercalate aromatic guests in a sandwich-type complex (89–95). In our case, the phenoxypropyl and chlorin heterodimer would represent a half-sandwich system, where chlorin–chlorin homodimers could be neglected as there are little to no interactions between the widely separated sensitizer molecules. Additional weak C–H... π interactions may also exist. Such pairing between the phenoxypropyl and sensitizer would further support the U shape of the sensitizer by bending to reach the phenoxypropyl site, which negatively impacting the sensitizer photorelease chemistry.

Summary

A photoreleasable sensitizer has been successfully synthesized and attached to silica using a chiral (1*S*,2*S*)-cyclohexane-1,2-dicarboxylate linker. The observed ~19-fold decrease in sensitizer loading, as compared to similar sensitizers bearing succinate or dimethylene linkers (55–58), can be attributed to a key problem. Namely, a bend in the *S,S*-linkage is found to hinder the sensitizer silane from coupling to the silica surface. Computations show the predominant form of the sensitizer trimer to be a U shape, which along with possible π - π stacking between the phenoxypropylsilane and the sensitizer, can account for the reduced efficiency of covalent bonding between the sensitizer and the silica surface.

Future prospective

The curved-sensitizer system we describe could possess an advantage where the sensitizer molecules are potentially resistant to aggregation (96). Otherwise, we find that the U shape of the system only leads to downsides (pun intended), which should be avoided. We learned from the study that the aromatic surface was not a good avenue to pursue. Alternative modifications that increase sensitizer departure from the surface are a more favorable venture. For example, Table 2 shows that the surface packing of the phenoxyxilanes and the fluorosilanes is nearly equal

and does not appear to be restrictive enough to account for the lower covalent bonding of the sensitizer. Therefore, the coverage was less dense than that of the fluorosilane functionalized silica, where the fluorosilanes promoted the sensitizer to adopt a vertical orientation by the repulsion of neighboring nonafluorosilanes. These nonafluorosilanes also yielded oxygen concentration increases, reduced $^1\text{O}_2$ quenching, and surface repelling properties that were advantageous in previous systems (41).

CONCLUSION

We have developed a five-step synthetic method to covalently attach a bent sensitizer linkage to a silica surface by a (*S,S*)-cyclohexyl bridge. As we saw, the resulting bend led to the less efficient covalent bonding of chlorin to silica. Co-doping of phenoxypropyl groups on the silica dampened the yield of alkene bond photocleavage by $^1\text{O}_2$.

One can anticipate that (*R,S*) and (*S,R*) to enable linear chiral orientations, while (*R,R*) will prompt diaxial substituent orientations, as we saw with the (*S,S*)-cyclohexyl. The attachment of other chiral groups to the surface, such as tartaric acid derivatives, has been seen for chiral surfaces for the tuning of enantiomer release kinetics. Retention of a perfluorinated surface, as we have used before, will also be beneficial.

These findings have led to our enhanced efforts to develop surfaces for $^1\text{O}_2$ and sensitizer delivery, including, $^1\text{O}_2$ -based sensitizer release reactions which we hope to take down new avenues. The (*S,S*)-cyclohexyl, dimethylene and succinate bridges we have synthesized will add to the array of linkages designed to understand how compounds release from photosensitive surfaces.

Our goal is to enable control over the linkage orientation, as well as other aspects of the bridge, in order to enhance sensitizer release. Modifying surfaces is an excellent way of revealing how drug photorelease can be tuned, which connects to how materials can be engineered for use in miniaturized photodynamic devices.

Acknowledgements—GG acknowledges support from the Beatrice Hunter Cancer Research Institute. GG and SAM acknowledge support from the Natural Sciences and Engineering Council of Canada, the Canadian Institutes of Health Research, the Canadian Foundation for Innovation, the Nova Scotia Research and Innovation Trust, and Acadia University. SAM acknowledges support from the National Cancer Institute of the National Institutes of Health under Award Number R01CA222227 (proviso: the content is solely the responsibility of the authors and does not necessarily represent the official views of the National Institutes of Health). SAM also acknowledges financial support from the University of North Carolina at Greensboro. GG, SJB, CC, NW, AAG and AG acknowledge support from the National Science Foundation (CHE-1464975). MV and AHT acknowledge support from the Agencia de Promoción Científica y Tecnológica (ANPCyT-Grant PICT-2015–1988). We acknowledge support from Consejo Nacional de Investigaciones Científicas y Técnicas (CONICET) and the National Science Foundation (NSF) through the Bilateral Cooperation Programme, Level I (PCB-I, Res.2172). EMG acknowledges support from the donors of the Petroleum Research Fund of the American Chemical Society, PSC-CUNY, the Eugene Lang Foundation at Baruch College. Computational support was provided by the Extreme Science and Engineering Discovery Environment (XSEDE), which is supported by the National Science Foundation Grant No. ACI01053575. We also thank Leda Lee for the graphic arts work.

SUPPORTING INFORMATION

Additional supporting information may be found online in the Supporting Information section at the end of the article:

- Figure S1.** ^1H NMR of compound **1** in CDCl_3 .
- Figure S2.** ^1H NMR of compound **2** in CDCl_3 .
- Figure S3.** ^{13}C NMR of compound **2** in CDCl_3 .
- Figure S4.** ^1H NMR of compound **3** in CDCl_3 .
- Figure S5.** ^{13}C NMR of compound **3** in CDCl_3 .
- Figure S6.** ^1H NMR of compound **4** in CDCl_3 .
- Figure S7.** ^1H NMR of compound **5** in CDCl_3 .
- Figure S8.** ^{13}C NMR of compound **5** in CDCl_3 .
- Figure S9.** Expanded ^1H NMR and ^1H - ^{13}C HSQC of compound **5** in CDCl_3 .
- Figure S10.** HRMS (+ESI) of compound **5**.
- Figure S11.** UV-vis spectrum of compound **5** in CHCl_3 .
- Figure S12.** Fluorescence spectrum of compound **5** in CHCl_3 .
- Figure S13.** UV-vis spectrum of compound **9** in *n*-butanol.

REFERENCES

1. Thum, M. D. and D. E. Falvey (2018) Photoreleasable protecting groups triggered by sequential two-photon absorption of visible light: Release of carboxylic acids from a linked anthraquinone-*N*-alkylpicolinium ester molecule. *J. Phys. Chem. A* **122**, 3204–3210.
2. Peterson, J. A., C. Wijesooriya, E. J. Gehrmann, K. M. Mahoney, P. P. Goswami, T. R. Albright, A. Syed, A. S. Dutton, E. A. Smith and A. H. Winter (2018) Family of BODIPY photocages cleaved by single photons of visible/near-infrared light. *J. Am. Chem. Soc.* **140**, 7343–7346.
3. Wang, X. and J. A. Kalow (2018) Rapid aqueous photouncaging by red light. *Org. Lett.* **20**, 1716–1719.
4. Dmitri, A., A. B. Romero and E. Ossipova (2018) Light-activatable prodrugs based on hyaluronic acid biomaterials. *Carbohydr. Polym.* **180**, 145–155.
5. Chitgupi, U., S. Shao, K. A. Carter, W.-C. Huang and J. F. Lovell (2018) Multicolor liposome mixtures for selective and selectable cargo release. *Nano Lett.* **18**, 1331–1336.
6. Slanina, T., P. Shrestha, E. Palao, D. Kand, J. A. Peterson, A. S. Dutton, N. Rubinstein, R. Weinstein, A. H. Winter and P. Klán (2017) In search of the perfect photocage: Structure-reactivity relationships in meso-methyl BODIPY photoremovable protecting groups. *J. Am. Chem. Soc.* **139**, 15168–15175.
7. Todorov, A. R., T. Wirtanen and J. Helaja (2017) Photoreductive removal of *O*-benzyl groups from oxyarene *N*-heterocycles assisted by *O*-pyridine–pyridone tautomerism. *J. Org. Chem.* **82**, 13756–13767.
8. Škalamera, D., V. B. Bregović, I. Antol, C. Bohne and N. Basarić (2017) Hydroxymethylaniline photocages for carboxylic acids and alcohols. *J. Org. Chem.* **82**, 12554–12568.
9. Chung, T. S., J. H. Park and M. A. Garcia-Garibay (2017) Triplet sensitized photodenitrogenation of Δ^2 -1,2,3-triazolines to form aziridines in solution and in the crystalline state: Observation of the triplet 1,3-alkyl-aminyl biradical. *J. Org. Chem.* **82**, 12128–12133.
10. Omlid, S. M., M. Zhang, A. Isor and R. D. McCulla (2017) Thiol Reactivity toward atomic oxygen generated during the photodeoxygenation of dibenzothiophene *S*-oxide. *J. Org. Chem.* **82**, 13333–13341.
11. Asad, N., D. Deodato, X. Lan, M. B. Widegren, D. L. Phillips, L. Du and T. M. Dore (2017) Photochemical activation of tertiary amines for applications in studying cell. *J. Am. Chem. Soc.* **139**, 12591–12600.
12. Walton, D. P. and D. A. Dougherty (2017) A general strategy for visible-light decaging based on the quinone trimethyl lock. *J. Am. Chem. Soc.* **139**, 4655–4658.
13. Chaudhuri, A., Y. Venkatesh, K. K. Behara and N. P. Singh (2017) Bimane: A visible light induced fluorescent photoremovable protecting group for the single and dual release of carboxylic and amino acids. *Org. Lett.* **19**, 1598–1601.
14. Abe, M., Y. Chitose, S. Jakkampudi, P. T. Thuy, Q. Lin, B. T. Van, A. Yamada, R. Oyama, M. Sasaki and C. Katan (2017) Design and synthesis of two-photon responsive chromophores for near-infrared light-induced uncaging reactions. *Synthesis* **49**, 3337–3346.
15. Madea, D., T. Slanina and P. Klán (2016) A ‘photorelease, catch and photorelease’ strategy for bioconjugation utilizing a *p*-hydroxyphenacyl group. *Chem. Commun.* **52**, 12901–12904.
16. Bari, I. D., R. Picciotto, G. Granata, A. R. Blanco, G. M. L. Consoli and S. Sortino (2016) A bactericidal calix[4]arene-based nanoconstruct with amplified NO photorelease. *Org. Biomol. Chem.* **14**, 8047–8052.
17. Šolomek, T., J. Wirz and P. Klán (2015) Searching for improved photoreleasing abilities of organic molecules. *Acc. Chem. Res.* **48**, 3064–3072.
18. Knoll, J. D., B. A. Albani and C. Turro (2015) New Ru(II) complexes for dual photoreactivity: Ligand exchange and $^1\text{O}_2$ generation. *Acc. Chem. Res.* **48**, 2280–2287.
19. Heymann, R. R., M. D. Thum, A. L. Hardee and D. E. Falvey (2017) Visible light initiated release of calcium ions through photochemical electron transfer reactions. *Photochem. Photobiol. Sci.* **16**, 1003–1008.
20. Kunsberg, D. J., A. H. Kipping and D. E. Falvey (2015) Visible light photorelease of carboxylic acids via charge-transfer excitation of *N*-methylpyridinium iodide esters. *Org. Lett.* **17**, 3454–3457.
21. Piloto, A. M., G. Hungerford, J. U. Sutter, M. S. Soares, P. G. Costa, M. Goncalves and T. Sameiro (2015) Photoactivatable heterocyclic cages in a comparative release study of butyric acid as a model drug. *J. Photochem. Photobiol., A* **299**, 44–53.
22. Bourdillon, M. T., B. A. Ford, A. T. Knulty, C. N. Gray, M. Zhang, D. A. Ford and R. D. McCulla (2014) Oxidation of plasmalogen, low-density lipoprotein and RAW 264.7 cells by photoactivatable atomic oxygen precursors. *Photochem. Photobiol.* **90**, 386–393.
23. Šebej, P., J. Wintner, P. Müller, T. Slanina, J. A. Anshori, L. P. Antony, P. Klán and J. Wirz (2013) Fluorescein analogues as photoremovable protecting groups absorbing at ~ 520 nm. *J. Org. Chem.* **78**, 1833–1843.
24. Callaghan, S. and M. O. Senge (2018) The Good, the bad, and the ugly – controlling singlet oxygen through design of photosensitizers and delivery systems for photodynamic therapy. *Photochem. Photobiol. Sci.* (in press, <https://doi.org/10.1039/c8pp00008e>).

25. Nani, R. R., A. P. Gorka, T. Nagaya, T. Yamamoto, J. Ivanic, H. Kobayashi and M. J. Schnermann (2017) In vivo activation of doxorubicin-antibody conjugates by near-infrared light. *ACS Cent. Sci.* **3**, 329–337.
26. Anderson, E. D., A. P. Gorka and M. J. Schnermann (2016) Near-Infrared uncaging or photosensitizing dictated by oxygen tension. *Nat. Commun.* **7**, 13378.
27. Gorka, A. P., R. R. Nani, T. Nagaya, H. Kobayashi and M. J. Schnermann (2016) Cyanine photocages enable the near-IR light activation of antibody-drug conjugates. *Angew. Chem. Int. Ed.* **54**, 13635–13638.
28. Nani, R. R., A. P. Gorka, T. Nagaya, H. Kobayashi and M. J. Schnermann (2015) Near-IR light-mediated cleavage of antibody-drug conjugates using cyanine photocages. *Angew. Chem. Int. Ed.* **127**, 13839–13842.
29. Pritam, T., M. Li, R. Karki, M. Bio, P. Rajaputra, G. Nkepong, S. Woo and Y. You (2017) Folate-peg conjugates of a far-red light-activatable paclitaxel prodrug to improve selectivity toward folate receptor-positive cancer cells. *ACS Omega* **2**, 6349–6360.
30. Pritam, T., M. Li, M. Bio, P. Rajaputra, G. Nkepong, Y. Sun, S. Woo and Y. You (2016) Far-red light-activatable prodrug of paclitaxel for the combined effects of photodynamic therapy and site-specific paclitaxel chemotherapy. *J. Med. Chem.* **59**, 3204–3214.
31. Bio, M., P. Rajaputra, G. Nkepong and Y. You (2014) Far-red light-activatable, multifunctional prodrug for fluorescence optical imaging and combinational treatment. *J. Med. Chem.* **57**, 3401–3409.
32. Nkepong, G., M. Bio, P. Rajaputra, S. G. Awuah and Y. You (2014) Folate receptor-mediated enhanced and specific delivery of far-red light-activatable prodrugs of combretastatin A-4 to FR-positive tumor. *Bioconjugate Chem.* **25**, 2175–2188.
33. Biswas, S., R. Mengji, S. Barman, V. Venugopal, A. Jana and N. P. Singh (2018) 'AIE + ESIP' assisted photorelease: Fluorescent organic nanoparticles for dual anticancer drug delivery with real-time monitoring ability. *Chem. Commun.* **54**, 168–171.
34. Ulbrich, K., K. Hola, V. Subr, A. Bakandritsos, J. Tucek and R. Zboril (2016) Targeted drug delivery with polymers and magnetic nanoparticles: Covalent and noncovalent approaches, release control, and clinical studies. *Chem. Rev.* **116**, 5338–5431.
35. Bao, C., L. Zhu, Q. Lin and H. Tian (2015) Building biomedical materials using photochemical bond cleavage. *Adv. Mater.* **27**, 1647–1662.
36. Couleaud, P., V. Morosini, C. Frochot, S. Richeter, L. Raehm and J. O. Durand (2010) Silica-based nanoparticles for photodynamic therapy applications. *Nanoscale* **2**, 1083–1095.
37. Tu, H. L., Y. S. Lin, H. Y. Lin, Y. Hung, L. W. Lo, Y. F. Chen and C. Y. Mou (2009) In vitro studies of functionalized mesoporous silica nanoparticles for photodynamic therapy. *Adv. Mater.* **21**, 172–177.
38. Carling, C., F. Nourmohammadian, J. Boyer and N. R. Branda (2010) Remote-control photorelease of caged compounds using near-infrared light and upconverting nanoparticles. *Angew. Chem. Int. Ed.* **49**, 3782–3785.
39. Wijtmans, M., S. J. Rosenthal, B. Zwanenburg and N. A. Porter (2006) Visible light excitation of CdSe nanocrystals triggers the release of coumarin from cinnamate surface ligands. *J. Am. Chem. Soc.* **128**, 11720–11726.
40. Qiuning, L., B. Chunyan, Y. Yunlong, L. Qiannan, Z. Dasheng, C. Shuiyu and Z. Linyong (2013) Highly discriminating photorelease of anticancer drugs based on hypoxia activatable phototrigger conjugated chitosan nanoparticles. *Adv. Mater.* **25**, 1981–1986.
41. Bartusik, D., D. Aebisher, G. Ghosh, M. Minnis and A. Greer (2012) Fluorine end-capped optical fibers for photosensitizer release and singlet oxygen production. *J. Org. Chem.* **77**, 4557–4565.
42. Huang, H., J. Yan, P. Liu, B. Zhao, Y. Cao and X. Zhang (2017) A novel cancer nanotheranostics system based on quantum dots encapsulated by a polymer-prodrug with controlled release behavior. *Aust. J. Chem.* **70**, 1302–1311.
43. Ardekania, S. M., A. Dehghani, M. Hassan, M. Kianinia, I. Aharonovich and V. G. Gomes (2017) Two-photon excitation triggers combined chemo-photothermal therapy via doped carbon nanohybrid dots for effective breast cancer treatment. *Chem. Eng. J.* **330**, 651–662.
44. Karthik, S., B. Saha, S. K. Ghosh and N. P. Singh (2013) Photoreversible quinoline tethered fluorescent carbon dots for regulated anticancer drug delivery. *Chem. Commun.* **49**, 10471–10473.
45. Ding, C., L. Tong, J. Feng and J. Fu (2016) Recent advances in stimuli-responsive release function drug delivery systems for tumor treatment. *Molecules* **21**, 1715.
46. Voliani, V., F. Ricci, G. Signore, R. Nifosi, S. Luin and F. Beltram (2011) Drug delivery: Multiphoton molecular photorelease in click-chemistry-functionalized gold nanoparticles. *Small* **7**, 3270.
47. Cheng, Y., T. L. Doane, C. H. Chuang, A. Ziady and C. Burda (2014) Near infrared light-triggered drug generation and release from gold nanoparticle carriers for photodynamic therapy. *Small* **10**, 1799–1804.
48. Qiu, H. and S. Che (2011) Chiral mesoporous silica: Chiral construction and imprinting via cooperative self-assembly of amphiphiles and silica precursors. *Chem. Soc. Rev.* **40**, 1259–1268.
49. Lynch, B., J. D. Glennon, C. Tröltzsch, U. Menyess, M. Pursch and K. Albert (1997) A (–)-menthyl bonded silica phase for chiral separations: Synthesis and solid state NMR characterization. *Anal. Chem.* **69**, 1756–1762.
50. Hisako, S., H. Yoshihisa, T. Kenji and Y. Akihiko (2005) Orientation tuning of a polypyridyl Ru(II) complex immobilized on a clay surface toward chiral discrimination. *J. Phys. Chem. B* **109**, 18935–18941.
51. Benitez, M., G. Bringmann, M. Dreyer, H. Garcia, H. Ihmels, M. Waidelich and K. Wissel (2005) Design of a chiral mesoporous silica and its application as a host for stereoselective di-*p*-methane rearrangements. *J. Org. Chem.* **70**, 2315–2321.
52. Clarke, R. J. and I. J. Shannon (2001) Mesopore immobilised copper bis(oxazoline) complexes for enantioselective catalysis. *Chem. Commun.* **19**, 1936–1937.
53. Guo, Z., Y. Du, X. Liu, S. C. Ng, Y. Chen and Y. Yang (2010) Enantioselectively controlled release of chiral drug (metoprolol) using chiral mesoporous silica materials. *Nanotechnology* **21**, 165103.
54. Li, J., X. Du, N. Zheng, L. Xu, J. Xu and S. Li (2016) Contribution of carboxyl modified chiral mesoporous silica nanoparticles in delivering doxorubicin hydrochloride in vitro: pH-response controlled release, enhanced drug cellular uptake and cytotoxicity. *Colloids Surf. B* **141**, 374–381.
55. Ghosh, G., M. Minnis, A. A. Ghogare, I. Abramova, K. A. Cengel, T. M. Busch and A. Greer (2015) Photoactive fluoropolymer surfaces that release sensitizer drug molecules. *J. Phys. Chem. B* **119**, 4155–4164.
56. Mahendran, A., Y. Kopkalli, G. Ghosh, A. Ghogare, M. Minnis, B. I. Krufft, M. Zamadar, D. Aebisher, L. Davenport and A. Greer (2011) A hand-held fiber-optic implement for the site-specific delivery of photosensitizer and singlet oxygen. *Photochem. Photobiol.* **87**, 1330–1337.
57. Bartusik, D., M. Minnis, G. Ghosh and A. Greer (2013) Autocatalytic-assisted photorelease of a sensitizer drug bound to a silica support. *J. Org. Chem. Soc.* **78**, 8537–8544.
58. Zamadar, M., G. Ghosh, A. Mahendran, M. Minnis, B. I. Krufft, A. Ghogare, D. Aebisher and A. Greer (2011) Photosensitizer drug delivery via an optical fiber. *J. Am. Chem. Soc.* **133**, 7882–7891.
59. Lorente, C., E. Arzoumanian, C. Castaño, E. Oliveros and A. H. Thomas (2014) A non-singlet oxygen mediated reaction photoinduced by phenalenone, a universal reference for singlet oxygen sensitization. *RSC Adv.* **4**, 10718.
60. Stewart, J. P. (2007) Optimization of parameters for semiempirical methods. V. Modification of NDDO approximations and application to 70 elements. *J. Mol. Model.* **13**, 1173–1213.
61. Frisch, M. J., G. W. Trucks, H. B. Schlegel, G. E. Scuseria, M. A. Robb, J. G. Scalmani, V. Barone, B. Mennucci, G. A. Petersson, H. M. Caricato, X. Li, H. P. Hratchian, A. F. Izmaylov, J. G. Zheng, J. L. Sonnenberg, M. Hada, M. Ehara, K. R. Fukuda, J. Hasegawa, M. Ishida, T. Nakajima, Y. Honda, O. H. Nakai, T. Vreven, J. A. Montgomery, J. E. Peralta, F. M. Bearpark, J. J. Heyd, E. Brothers, K. N. Kudin, V. N. Staroverov, R. Kobayashi, J. Normand, K. Raghavachari, A. Rendell, J. C. Burant, S. S. Iyengar, J. Tomasi, M. Cossi, N. M. Millam, M. Klene, J. E. Knox, J. B. Cross, V. Bakken, C. A. Jaramillo, R. Gomperts, R. E. Stratmann, O. Yazyev, A. J. Austin, R. Cammi, C. Pomelli, J. W. Ochterski, R. L. Martin, K. Morokuma, V. G. Zakrzewski, G. A. Voth, P. Salvador, J. J. Dannenberg, S. Dapprich, A. D. Daniels, O. Farkas, J. B. Foresman, J. V. Ortiz, J. Cioslowski and D. J. Fox (2009) *Gaussian 09, Revision D01*. Gaussian Inc., Wallingford, CT.

62. Stewart, J. P. (2009) Application of the PM6 method to modeling proteins. *J. Mol. Model.* **15**, 765–805.
63. Dennington, R., T. Keith and J. Millam (2009) *GaussView 5*. Semichem Inc, Shawnee, Mission KS.
64. Wongsinkongman, P., A. Brossi, H. Wang, K. F. Bastow and K. Lee (2002) Antitumor agents. Part 209: Pheophorbide-a derivatives as photo-independent cytotoxic agents. *Bioorg. Med. Chem.* **10**, 583–591.
65. Li, J., X. Zhang, Y. Liu, I. Yoon, D. K. Kim, J. G. Yin, J. J. Wang and Y. K. Shim (2015) Synthesis, optical properties and preliminary in vitro photodynamic effect of pyridyl and quinoxalyl substituted chlorins. *Bioorg. Med. Chem.* **23**, 1684–1690.
66. Pavlov, V. Y., I. O. Konstantinov, G. V. Ponomarev, V. P. Timofeev and B. G. Kimel (2005) Synthesis of new derivatives of protoporphyrin IX and chlorophyll-a. *Russ. J. Org. Chem.* **41**, 1824–1835.
67. Neises, B. and W. Steglich (1978) Simple method for the esterification of carboxylic acids. *Angew. Chem. Int. Ed.* **17**, 522–524.
68. Chou, T., K. Liao and J. Lin (2005) Synthesis and luminescence properties of U-shaped polycyclic molecules containing *syn*-facial functionalized quinoxaline rings. *Org. Lett.* **7**, 4843–4846.
69. Gleiter, R. and W. Schaefer (1990) Interactions between nonconjugated π -systems. *Acc. Chem. Res.* **23**, 369–375.
70. Klärner, F. and B. Kahlert (2013) Molecular tweezers and clips as synthetic receptors. Molecular recognition and dynamics in receptor–substrate complexes. *Acc. Chem. Res.* **36**, 919–932.
71. Rebek, J. (1999) Reversible encapsulation and its consequences in solution. *Acc. Chem. Res.* **32**, 278–286.
72. Vasudevan, S. R., J. B. Moore, Y. Schymura and G. C. Churchill (2012) Shape-based reprofiling of FDA-approved drugs for the H₁ histamine receptor. *J. Med. Chem.* **55**, 7054–7060.
73. Lu, J., S. Patel, N. Sharma, S. M. Soisson, R. Kishii, M. Takei, Y. Fukuda, K. J. Lumb and S. B. Singh (2014) Structures of kbidelomycin bound to staphylococcus aureus GyrB and ParE showed a novel U-shaped binding mode. *ACS Chem. Biol.* **9**, 2023–2031.
74. Ando, T., M. Ota, T. Kashiwagi, N. Nagashima, Y. Ariyoshi, R. K. Chadha, T. Yamazaki and M. Goodman (1993) Absolute configurations and conformations of sweet and tasteless aminomalonyl (Ama) dipeptide esters: Ama-Phe-OMe and Ama-Phe-OEt. *J. Am. Chem. Soc.* **115**, 397–402.
75. Wercholak, A. N., J. M. Thuman, J. L. Stanley, A. L. Sargent, E. S. Anderson and W. E. Allen (2016) Incorporation of fluorophore-cholesterol conjugates into liposomal and mycobacterial membranes. *Bioorg. Med. Chem.* **24**, 1045–1049.
76. Clarke, R. J. and I. J. Shannon (2001) Mesopore immobilised copper bis(oxazoline) complexes for enantioselective catalysis. *Chem. Commun.* **19**, 1936–1937.
77. Mishra, G. S., A. Kumar and P. B. Tavares (2012) Single site anchored novel Cu(II) catalysts for selective liquid-gas phase O₂ oxidation of *n*-alkanes. *J. Mol. Catal. A* **357**, 125–132.
78. Kesanli, B. and W. Lin (2004) Mesoporous silica anchored Ru catalysts for highly enantioselective hydrogenation of beta-ketoesters. *Chem. Commun.* **20**, 2284–2285.
79. Mello, R., A. Olmos, T. Varea and E. Gonza (2008) Analysis of hybrid silica materials with the aid of conventional NMR and GC/MS. *Anal. Chem.* **80**, 9355–9359.
80. Marans, N. S. and L. H. Sommer (1951) Preparation of organofluorosilanes using aqueous hydrofluoric acid. *J. Am. Chem. Soc.* **73**, 5127–5130.
81. Boix-Garriga, E., B. Rodriguez-Amigo, O. Planas and S. Nonell (2016) Properties of singlet oxygen. In *Singlet Oxygen: Applications in Biosciences and Nanosciences* (Edited by S. Nonell and C. Flors), pp. 1–450. Royal Society of Chemistry (RSC), Abingdon, Oxfordshire, UK.
82. Stallivieri, A., F. Baros, P. Arnoux, R. Vanderesse, M. Barberi-Heyob and C. Frochot (2016) Production of singlet oxygen by nanoparticle-bound sensitizers. In *Singlet Oxygen: Applications in Biosciences and Nanosciences* (Edited by S. Nonell and C. Flors), pp. 209–223. Royal Society of Chemistry (RSC), Abingdon, Oxfordshire, UK.
83. Wilkinson, F., W. P. Helman and A. B. Ross (1995) Rate constants for the decay and reactions of the lowest electronically excited singlet state of molecular oxygen in solution. An expanded and revised compilation. *J. Phys. Chem. Ref. Data* **24**, 663–1021.
84. Baugh, S. D. P., Z. Yang, D. K. Leung, D. M. Wilson and R. Breslow (2001) Cyclodextrin dimers as cleavable carriers of photodynamic sensitizers. *J. Am. Chem. Soc.* **123**, 12488–12494.
85. Ruebner, A., Z. Yang, D. Leung and R. Breslow (1999) A cyclodextrin dimer with a photocleavable linker as a possible carrier for photosensitizer in photodynamic tumor therapy. *Proc. Natl Acad. Sci. USA* **96**, 14692–14693.
86. Murthy, R. S., M. Bio and Y. You (2009) Low energy light-triggered oxidative cleavage of olefins. *Tetrahedron Lett.* **50**, 1041–1044.
87. Dinache, A., A. Smarandache, A. Simon, V. Nastasa, T. Tozar, A. Pascu, M. Enescu, A. Khatyr, F. Sima, M.-L. Pascu and A. Staicu (2017) Photosensitized cleavage of some olefins as potential linkers to be used in drug delivery. *Appl. Surf. Sci.* **417**, 136–142.
88. Erden, I., P. E. Alscher, J. R. Keeffe and C. Mercer (2005) Dye-sensitized photooxygenation of the C=N Bond. 5. Substituent effects on the cleavage of the C=N bond of C-aryl-N-aryl-N-methylhydrazones. *J. Org. Chem.* **70**, 4389–4392.
89. Ehrlich, S., J. Moellmann and S. Grimme (2013) Dispersion-corrected density functional theory for aromatic interactions in complex systems. *Acc. Chem. Res.* **46**, 916–926.
90. Ema, T., N. Ura, K. Eguchi, Y. Ise and T. Sakai (2011) Chiral porphyrin dimer with a macrocyclic cavity for intercalation of aromatic guests. *Chem. Commun.* **47**, 6090–6092.
91. Elguero, J., I. Alkorta, R. M. Claramunt, C. López, D. Sanz and D. S. María (2009) Theoretical calculations of a model of NOS indazole inhibitors: Interaction of aromatic compounds with Zn-porphyrins. *Bioorg. Med. Chem.* **17**, 8027–8031.
92. Feng, D., G. Wang, J. Wu, R. Wang and Z. Li (2007) Hydrogen bonding-driven elastic bis(zinc)porphyrin receptors for neutral and cationic electron-deficient guests with a sandwich-styled complexing pattern. *Tetrahedron Lett.* **48**, 6181–6185.
93. Haino, T., T. Fujii and Y. Fukazaw (2006) Guest binding and new self-assembly of bisporphyrins. *J. Org. Chem.* **71**, 2572–2580.
94. Hunter, C. A. and J. M. Sanders (1990) The nature of π - π interactions. *J. Am. Chem. Soc.* **112**, 5525–5534.
95. Añez, R., A. Sierralta, D. Coll, O. Castellanos and H. Soscund (2016) Moller-Plesset 2 and density functional theory studies of the interaction between aromatic compounds and Zn-porphyrins. *Comput. Theor. Chem.* **1084**, 133–139.
96. Uchoa, A. F., K. T. de Oliveira, M. S. Baptista, A. J. Bortoluzzi, Y. Iamamoto and O. A. Serra (2011) Chlorin photosensitizers sterically designed to prevent self-aggregation. *J. Org. Chem.* **76**, 8824–8832.